Spatially and temporally variable sulfur cycling in shallow-sea hydrothermal vents, Milos, Greece

Jennifer L. Houghton[a],[*], William P. Gilhooly III[b], Fotios-Christos A. Kafantaris[c], Gregory K. Druschel[b], Guang-Sin Lu[d], Jan P. Amend[d],[e], Athanasios Godelitsas[f], David A. Fike[a],[*]

[a] Dept. of Earth and Planetary Sciences, Washington University, St. Louis, MO, USA
[b] Dept. of Earth Sciences, Indiana University-Purdue University Indianapolis, Indianapolis, IN, USA
[c] Department of Crop and Soil Sciences, North Carolina State University, Raleigh, NC, USA
[d] Dept. of Earth Sciences, University of Southern California, Los Angeles, CA, USA
[e] Dept. Biological Sciences, University of Southern California, Los Angeles, CA, USA
[f] Dept. of Geology and Geoenvironment, National and Kapodistrian University of Athens, Athens, Greece

ARTICLE INFO

ABSTRACT

Shallow-sea hydrothermal systems are ideal for studying the relative contributions to sedimentary sulfur archives from ambient sulfur-utilizing microbes and from fluxes of hydrothermally derived sulfur. Here we present data from a vent field in Palaeochori Bay, Milos, Greece using a suite of biogeochemical analytical tools that captured both spatial and temporal variability in biotic and abiotic sulfur cycling. Samples were collected along a transect from a seagrass meadow to an area of active venting. The abundance and isotopic composition of sulfide captured in situ, together with geochemistry from sedimentary porewaters and the overlying water column and solid phase sulfide minerals, record evidence of ephemeral activity of microbial sulfate reduction as well as sulfide oxidation. The sulfur and oxygen isotope composition of porewater sulfates indicate active sulfate reduction within the transition zone between the vents and seagrass, rapid recycling of biologically produced sulfide within non-vent sediments, and reoxidation of abiotic sulfide within the vent field. A phylogenetic survey of sediments also indicates the pervasive presence of a suite of putative sulfur-metabolizing bacteria, including sulfate reducers and sulfide oxidizers, many of which can utilize intermediate valence sulfur compounds. The isotopic composition of pyrite in these sediments consistently records a microbially influenced signature ($\delta^{34}S_{py}$ of -4.4 to $-10.8‰$) relative to the hydrothermal endmember ($\delta^{34}S \sim +2.5‰$), independent of distance from the vent source. The narrow range of pyrite $\delta^{34}S$ across sediments with a highly variable hydrothermal influence suggests that physical mixing (e.g., by storm events) homogenizes the distribution of biogenic and hydrothermal Fe-sulfides throughout the region, overprinting the spatially and temporally variable interplay between biological and hydrothermal sulfur cycling in these environments.

1. Introduction

Sulfur cycling in marine sedimentary environments is a complex network of connected biotic and abiotic reactions driven largely by the marine sulfate reservoir as the ultimate sulfur source. These processes transform sulfur phases between the oxidized (sulfate) and reduced (sulfide) end members, along with numerous intermediate valence compounds (e.g., polysulfides, elemental sulfur, thiosulfate, sulfite) (Fike et al., 2015). These reactions are intimately linked and the sulfur cycle becomes more complex in areas of hydrothermal activity characterized by the advective influx of reduced sulfur species (e.g. Wenzhöfer et al., 2000). The interfaces between biotic and abiotic

(hydrothermal) processes in such settings can be investigated in shallow-sea hydrothermal systems (Price et al., 2013; Gilhooly et al., 2014; Meyer-Dombard et al., 2013; Akerman et al., 2011; Rusch and Amend, 2008).

Milos is a volcanic island in the Aegean Sea that lies along the Hellenic Volcanic Arc (e.g. Fytikas et al., 1986; Nomikou et al., 2013) surrounded by accessible shallow-sea hydrothermal systems (e.g. Dando et al., 1995; Varnavas and Cronan, 2005; Valsami-Jones et al., 2005; Fig. 1 inset). Abundant shallow-sea (5–20 m depth) hydrothermal venting in Palaeochori Bay, located off southeastern Milos, manifests both as areas of free gas discharge and diffusively venting geothermal fluids (e.g., Dando et al., 1995). Hydrogen sulfide is abundant both in
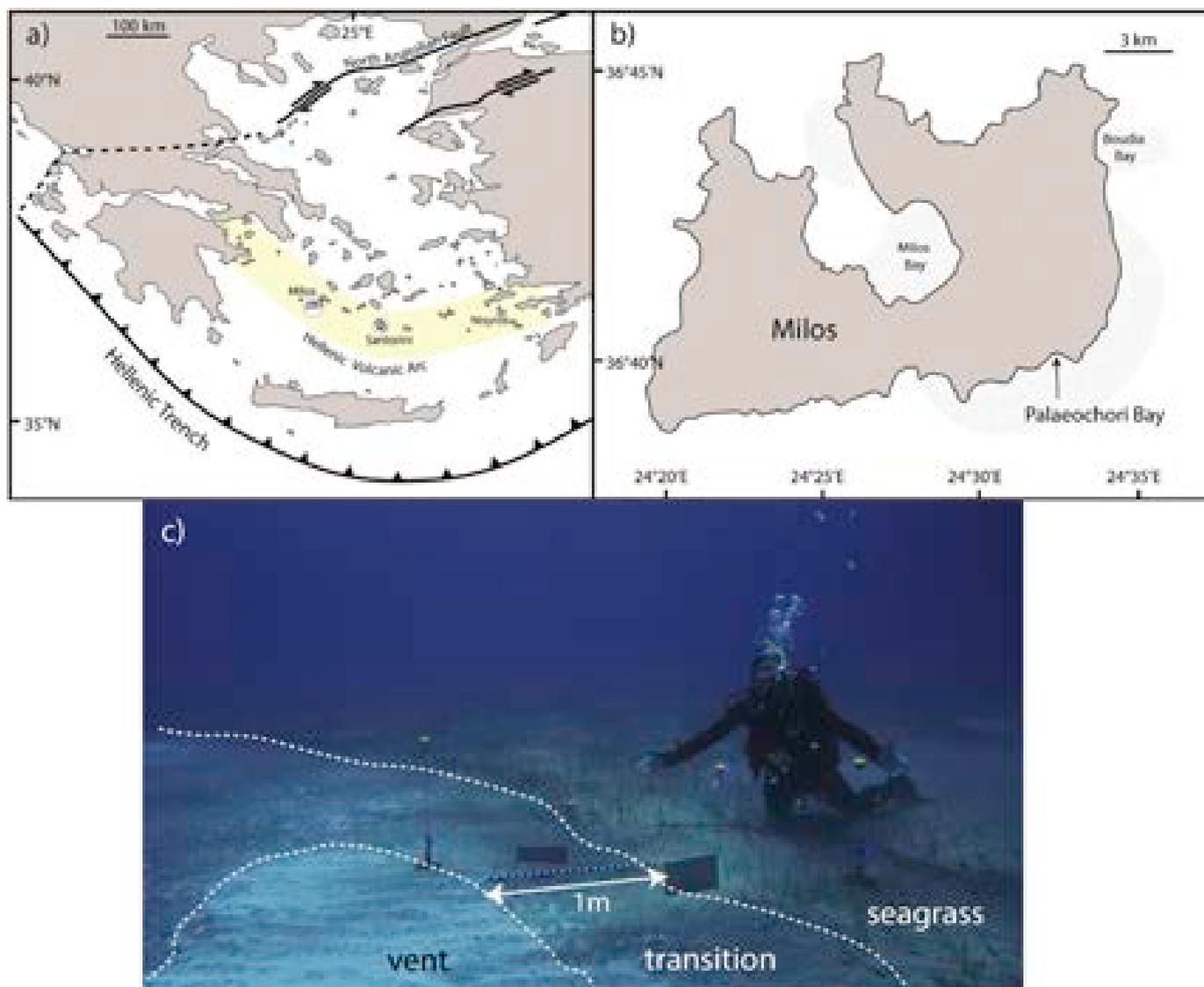

Fig. 1. (a) Location of Milos within the Hellenic Volcanic Arc (in yellow). Samples for this study were taken in shallow water within hydrothermally active sediments in Palaeochori Bay (b) across a transect from the venting source to more distal seagrass patches (c). A 1-m bar is in the photo for scale. Background sediment samples were taken 50 m away from any evidence of hydrothermal activity, outside of the field of view in the photo. (For interpretation of the references to colour in this figure legend, the reader is referred to the web version of this article.)

free gas (up to 5 vol%) as well as in the hydrothermal fluids (up to several millimolar). Ongoing sulfur cycling has been well studied in Palaeochori Bay where hydrothermal activity has been observed to vary strongly on short spatial and temporal scales (Wenzhöfer et al., 2000; Yücel et al., 2013; Gilhooly et al., 2014; Fike et al., 2017), suggesting a complex patchwork of abiotic and biotic processes in the area. Here we seek to investigate how this interplay between abiotic hydrothermal activity and microbial sulfur cycling impacts the generation and preservation in the sediments of stable isotopic signatures diagnostic for various biological and environmental processes.

In this environment, sulfide from reduced, H_2S-rich hydrothermal fluids and produced by microbial sulfate reduction from ambient seawater together support a diverse population of sulfide oxidizing bacteria (Sievert et al., 1999) and lead to the precipitation of crystalline and amorphous sulfide minerals (Dando et al., 1999; Varnavas and Cronan, 2005; Pichler et al., 1999; Price et al., 2013; Godelitsas et al., 2015). Moreover, given that sulfide can be sourced either from hydrothermal fluids (abiogenic) or from the product of microbial sulfate reduction, these shallow sediments are ideal for investigating the interface(s) between abiotic and biotic regimes, distinguishable by the

stable sulfur isotopic composition of sulfide. Furthermore, because these systems are driven by advective hydrothermal fluid flow, in-situ sampling of sulfide is essential to faithfully document environmental conditions; the recovery and subsequent geochemical analysis of core samples (even on-shore immediately after collection) can result in spurious results (i.e., those not present in situ) because of the loss of advective flow through the sediments.

Previous work has documented the abundance and isotopic composition of hydrogen sulfide in Palaeochori hydrothermal fluids and sedimentary porewaters (Gilhooly et al., 2014). From these results, it appeared that the H_2S analyzed in porewaters near several vent sources had a narrow $\delta^{34}S$ distribution ($+2.7‰ \pm 0.4‰$), consistent with a single hydrothermal source. The local $\delta^{34}S$ composition of the seawater sulfate overlying these sites of venting was also found to have decreased, consistent with a substantial contribution to the ambient sulfate pool from the oxidation of hydrothermal H_2S (Gilhooly et al., 2014). In May 2014, field sampling was conducted along a lateral transect from vent source to background sediments in a vent field referred to here as Saganaki in Palaeochori Bay (Fig. 1). The sediment surface is marked by abundant cm-scale wave ripples and intermittently
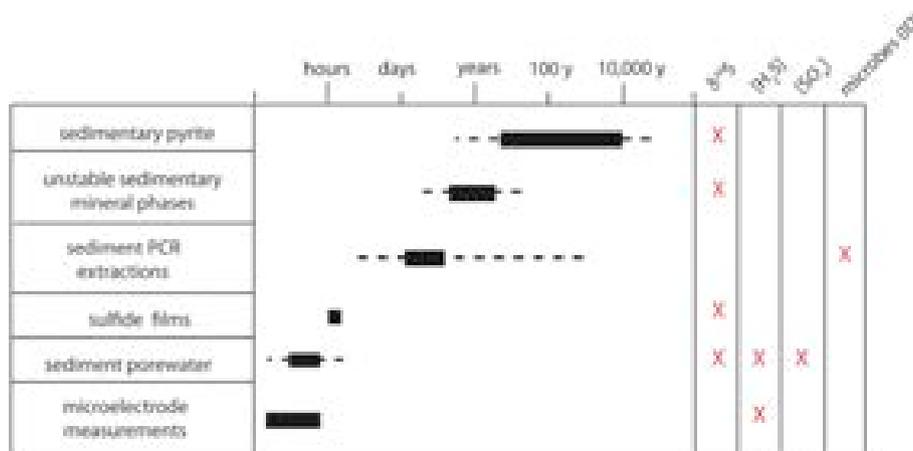
Fig. 2. The sample type and measurement technique capture temporally averaged signals, each integrating over different timescales.

covered with white and yellow mineral patches and small mounds of dark, fluidized sand associated with free gas discharge. These white and yellow patches tend to be significantly warmer ($> 70\,°C$) than the surrounding sediments. In addition to this hydrothermal activity, there are isolated stands of sea grass and associated pockets of organic matter accumulation that are likely to drive microbial sulfate reduction, as observed in diversity surveys of the sediments. A variety of geochemical and microbiological sampling techniques were deployed to capture environmental conditions averaged over a range of temporal and spatial scales (Fig. 2). Repeated sample collections over several days allowed an investigation of temporal variability in the sulfur cycling patterns in this system. Using this interdisciplinary sampling approach, the relative contributions from hydrothermal (abiotic) and microbial processes to various aqueous and sedimentary geochemical phases can be assessed.

2. Methods

2.1. Field sampling and preservation of sediments and porewater

Cores were collected from the subsurface by a team of scuba divers. Sample locations are divided into distinct environments based on visual transitions on the seafloor: vent sediments are covered in a characteristic white layer, the transition zone lacks any visible precipitate and also has no evidence of bioturbation, while the seagrass area is disturbed by bioturbation (Fig. 1c). Temperature and pH of porewater and overlying water column were recorded in the field. Immediately upon collection, cores were brought back to the beach and processed on shore as described. Porewaters were extracted from sediment cores using $0.2\,\mu m$ rhizons (Rhizosphere Research Products) inserted every 2 cm. Sediments were then subsampled every 2 cm, corresponding to rhizon placement and preserved frozen on dry ice prior to storage at $-80\,°C$. In parallel, porewaters were also extracted in situ from a range of locations using 60 mL syringes with a modified tapered nozzle with filter to exclude sediments; these fluids were collected at depth intervals of 5 cm and subsequently filtered with $0.2\,\mu m$ filters. The dissolved sulfide from vent fluids was sampled in situ either by capturing free gas bubbling from sediments by allowing gas to displace background seawater in serum bottles inverted over the sediment-water interface or by drawing 30 mL of fluid sample into a gas-tight syringe and later adding 20 mL of N_2 headspace. Porewater dissolved sulfide was precipitated as zinc sulfide (ZnS) by addition of 5% zinc acetate (wt./vol.) in the field and stored refrigerated prior to analysis.

2.2. Chemical analysis of porewater

An aliquot (1 mL) of each water sample fixed with zinc acetate was analyzed for sulfide concentration using the Cline (1969) method,

diluted as needed to be in range of standards. The remainder was centrifuged and the supernatant removed for further analysis. The ZnS solid was rinsed, dried, and weighed for isotopic analysis. An aliquot of the supernatant (~1 mL) was analyzed for major anions (F^-, Cl^-, Br^-, NO_3^-, PO_4^{3-}, SO_4^{2-}) by IC (Metrohm 881, USA) using an A-Supp-5 column with 3.2 mM Na_2CO_3/1 mM $NaHCO_3$/2.5% acetone eluent (Wilson et al., 2011). Anions were quantified after suppression using a conductivity detector. Excess 1 M $BaCl_2$ was added to the remaining supernatant to precipitate aqueous sulfate as barium sulfate ($BaSO_4$). The resulting $BaSO_4$ solid was rinsed, dried, and weighed for sulfur and oxygen isotopic analysis.

2.3. Sulfide film deployment and extraction

Photo film (ISO 100, Ilford, UK) was pre-soaked in MQ water prior to use in the field to remove photographic dyes. Care was taken to protect films from light prior to and after field exposures. In the field, sulfide films were taped to thin metal plates and pushed into sediments for either 4–6 h (daytime) or 16 h (overnight) exposures. The recovered films were rinsed with water and allowed to dry before storing until extraction in the laboratory. A portion of each film was cut into 0.5–1.0 cm sections with depth, depending on the amount of sulfide as determined by the darkness of the film. Extraction of sulfide from each section of film was performed following the protocol in Fike et al. (2017) using zinc acetate traps. Film yield was determined by measuring the concentration of ZnS in each trap using the Cline method on an aliquot (1 mL) of trap solution, diluted as needed to be in range of standards (Cline, 1969). The remainder of the trap solution was quantitatively converted to sulfate using 30% peroxide and dilute HCl and subsequently fixed with 1 M $BaCl_2$ (Fike et al., 2017). Oxidizing the zinc sulfide was found to produce a higher solid yield (due to zinc sulfide complexes) and to combust more reliably during isotopic analysis. The $BaSO_4$ yield was rinsed, dried, and weighed for sulfur isotopic analysis.

2.4. Sediment extractions

Aliquots of each previously frozen sediment subsample (taken every 2-cm with depth) were weighed while frozen and immediately extracted for bulk chromium-reducible sulfur (CRS) following the method of Canfield et al. (1986). Briefly, this extracts all Fe-sulfides occurring in the sediment (mainly pyrite, but also mackinawite- and greigite-type phases) as well as elemental sulfur using 6 N HCl and 1 M reduced chromium chloride under a N_2 atmosphere, using the N_2 to pass the evolved H_2S gas through a water trap into a zinc acetate trap (0.1 M) to precipitate ZnS.

A separate frozen aliquot was weighed and rinsed 3 times in dichloromethane (DCM) to extract elemental sulfur. The DCM extract was

evaporated to dryness at room temperature and the residue collected for sulfur isotopic analysis. The extracted sediments were allowed to air dry before conducting a second sequential extraction with 6 N HCl under N_2, trapping evolved H_2S as ZnS as described above, to extract any acid-volatile sulfur (AVS; Rickard and Morse, 2005), which includes reduced sulfur mineral phases (e.g., mackinawite and greigite; Rickard and Luther, 2007). Following this sequential treatment, the remaining sediments were rinsed 3 times with DI water prior to performing a CRS extraction to isolate the remaining pyrite. If the CRS extraction could not be conducted immediately, the rinsed sediments were stored at $-80\,°C$.

2.5. Stable isotopes

Samples preserved as barium sulfate or zinc sulfide were homogenized prior to weighing ~300 μg into tin capsules, along with excess V_2O_5 for barite samples. The sulfur isotope composition ($\delta^{34}S$) was analyzed on a Thermo Delta V Plus IRMS following online combustion with a coupled Costech ECS 4010 Elemental Analyzer at Washington University in St. Louis. The sulfur isotope value of the sample is expressed in standard delta notation as per mil (‰) deviations from Vienna Canyon Diablo Troilite (V-CDT). Isotopic measurements were calibrated against 3 in-house standards that have been calibrated against international standards IAEA-S-1 ($\delta^{34}S = -0.3‰$), IAEA-S-3 ($\delta^{34}S = -32.55‰$), and NBS-127 ($\delta^{34}S = +21.1‰$), with analytical errors of $< 0.3‰$ (1σ) for $\delta^{34}S$.

The oxygen isotope composition of barium sulfate ($\delta^{18}O_{SO4}$) was determined by high-temperature pyrolysis (at 1450 °C) on a Thermo TCEA coupled to a Thermo Delta V Plus at Indiana University-Purdue University Indianapolis. Approximately 100 μg of sample was weighed into a silver cup with an equal amount of graphite to promote instantaneous pyrolysis. Isotope data were normalized to Vienna Standard Mean Ocean Water (VSMOW) by regression of international reference materials NBS-127 ($\delta^{18}O = 8.59‰$), IAEA-SO5 ($\delta^{18}O = 12.13‰$), and IAEA-SO6 ($\delta^{18}O = -11.35‰$). Analytical precision for each standard was $< 0.2‰$ (1σ) and replicate analyses of three different samples were within 0.0 to 0.2‰.

A set of mass balance equations were used to determine the relative influence of sulfate reduction and sulfide oxidation on the isotopic variability observed in Milos porewaters. The relative contribution of oxidized sulfide within the highly advective vent sediments was estimated using the mass balance model:

$$\delta^{34}S_{pw} = \delta^{34}S_{sw}f_{sw} + (\delta^{34}S_{H_2S} + \mathcal{E}^{34}S_{SO_4-H_2S})(1 - f_{sw}) \qquad (1)$$

where the sulfur isotope composition of the porewater (pw) sulfate is a mixture of the fractional abundance (f) of Milos seawater (sw) sulfate ($\delta^{34}S \sim 22‰$; see results) and sulfate produced during the oxidation of porewater sulfide ($\delta^{34}S_{H_2S} \sim -12‰$; see results) offset by the isotope fractionation ($\mathcal{E}^{34}S_{SO_4-H_2S} = -5.2‰$; Fry et al., 1988) during abiotic oxidation of hydrogen sulfide by molecular oxygen. Using a similar equation, the relative contribution of sulfate produced during sulfide oxidation was calculated according to

$$\delta^{18}O_{pw} = \delta^{18}O_{sw}f_{sw} + (\delta^{18}O_{H_2O} + \mathcal{E}^{18}O_{SO_4-H_2O})(1 - f_{sw}) \qquad (2)$$

where the oxygen isotope composition of porewater sulfate is a mixture of Milos seawater sulfate ($\delta^{18}O = 9‰$) and oxygen derived from ocean water ($\delta^{18}O = 1.1‰$; Price et al., 2013). The fractionation in oxygen that occurs during the oxidation of hydrogen sulfide is not presently characterized in the literature. We assume this offset is similar to the fractionation observed between sulfate and water during abiotic pyrite oxidation ($\mathcal{E}^{18}O_{SO_4-H_2O} = 4‰$; Balci et al., 2007). The combined solutions of Eqs. (1) and (2) establish a mixing array between oxidized sulfide and seawater sulfate.

2.6. DNA extraction and bioinformatic analysis

Bulk environmental DNA was extracted from frozen sediment (at 10 cm depth) and porewater samples within 15 days of collection using the method of Mills et al. (2012). Each sediment sample (~0.5 g) and porewater sample (0.5 L filtered through 47 mm, 0.2 μm Supor filters (Pall Corporation, Port Washington, USA)) was separately homogenized using a sterile mortar and pestle. Optical densities of DNA extracts were measured using a NanoDrop ND-1000 spectrophotometer. Negative controls confirmed that there were no contaminating nucleic acids during sample collection or the DNA extraction process. Extracted DNA samples were sequenced by Molecular Research DNA (Shallowater, TX, USA) with recommended reagents, following manufacturer's guidelines. 16S rDNA assays were sequenced on an Illumina Miseq platform with universal primers 515 forward and 806 reverse (Caporaso et al., 2011), producing amplicons of the V4 hypervariable region. Sequence and diversity analyses were performed using the programs QIIME (version 1.9.0; Caporaso et al., 2010) and Mothur (version 1.37.2; Schloss et al., 2009) and compared against SILVA119 database (operational taxonomic units (OTUs) with a 97% identity). Sequences shorter than 200 bp, longer than 400 bp, and those that did not exactly match proximal primers were removed. Putative sulfur metabolisms and other physiologies were assigned based on the lowest blast level of published representative isolates in Bergey's Manual of Systematic Bacteriology, The Prokaryotes: A Handbook on the Biology of Bacteria, and in recent publications of newly defined species.

2.7. Voltammetry

In-situ voltammetric analysis was accomplished using an Analytical Instrument Systems, Inc. In-situ Electrochemical Analyzer (ISEA) unit. The ISEA includes a potentiostat housed in an aluminum case with watertight connectors for up to 8 working electrodes connected via a multiplexer to analyze in sequence (not simultaneously), with a single reference and a single counter electrode. The ISEA runs on internal batteries and is pre-programmed to run 10 scans for each working electrode, each electrode thus collects data in turn over approximately a 10-min cycle – yielding data for each spatial point every 10 min. The working electrodes consist of 100 μm diameter Au-amalgam electrodes, combined with a Ag/AgCl reference electrode and Platinum counter electrode (after Brendel and Luther, 1995). These electrodes can measure a range of electrochemically active analytes including most sulfur compounds (sulfide, polysulfide, elemental sulfur, thiosulfate, polythionates, and bisulfite; Druschel et al., 2004; Rozan et al., 2000), oxygen, iron, and manganese (Luther et al., 2008). Electrodes were calibrated against manganese (after the pilot ion method, Slowey and Marvin-Dipasquale, 2012) in the field, providing calibrations for sulfide, oxygen, and manganese. Elemental sulfur is a more complex signal and cannot be quantitatively calibrated, but changes in signal intensity do indicate changes in elemental sulfur concentrations and/or surface area and surface character conditions of particulates (Kafantaris, 2017). Six working electrodes were placed by SCUBA divers at the study sites, two in each of the 3 zones, each at two different depths, and run in a continual loop where each electrode was cycled every 10 min for a day. One of the working electrodes in the seagrass at 5 cm depth experienced a wiring failure and did not collect useable data. The reference and counter electrodes were placed in the water column near the working electrodes.

3. Results

3.1. Sediment porewater chemistry

The chloride and sulfate concentrations of Palaeochiori porewaters generally fall along a mixing line between the seawater and the sampled vent fluids, with more vapor-rich (e.g., low chloride) fluids nearest the

vent source transitioning to seawater concentrations with distance (Fig. S1a). The vapor-rich vent fluids sampled in the Saganaki vent field are consistent with phase separation and segregation at depth (Pichler et al., 1999; Price and Giovannelli, 2017). The isotopic composition of porewater sulfate nearest the vent source tends to be depleted in ^{34}S relative to seawater (Fig. 3a); however, the $\delta^{18}O_{SO4}$ values are either similar or higher than those in seawater (Fig. 4b). In contrast, the $\delta^{34}S_{SO4}$ and $\delta^{18}O_{SO4}$ values of porewaters in the transition zone tend to be higher than those in seawater (Fig. 3a; Fig. 4b). The $\delta^{34}S_{SO4}$ values of porewater sulfate in sediments beneath seagrass stands are isotopically indistinguishable from $\delta^{34}S_{SO4}$ of porewaters in distal sediments that are unaffected by hydrothermal activity (Fig. 3a). However, the oxygen isotope composition of porewater sulfate extracted from seagrass and background sediments ($\delta^{18}O_{SO4} = 8.8 \pm 0.22$‰; $n = 33$) both tend to be lower than ambient seawater sulfate (Fig. 4b).

Sulfide concentrations in porewaters in the top 20 cm are negligible beneath seagrass stands and in distal background sediments (Fig. S1b). Hydrogen sulfide abundance is inversely proportional to ambient pH, with measurable concentrations at pH < 6, found only in the top 20 cm of sediments near the vent and in the transition zone (Fig. S1b). Sulfide $\delta^{34}S$ in porewaters nearest the vent source, at least on these sampling days, are similar to the endmember vent fluid composition (Fig. 3b). Porewater composition provides a snapshot of microbial activity in these advective systems temporally averaged over minutes to hours (Fig. 2).

3.2. Isotopic composition of the sediment record

Sediments were analyzed for bulk CRS (capturing and integrating pyrite, elemental S, and monosulfides) as well as with a sequential extraction for elemental sulfur, AVS (i.e., monosulfides), and then CRS (here just targeting pyrite) to assess the relative abundance of these individual phases. The yield of bulk sediment CRS was almost always significantly higher than that of CRS (i.e. pyrite) in sequentially extracted sediments (Table 1). The cases where pyrite yield exceeds the bulk CRS yield are likely due to variability between aliquots of sediment, as the sediments were subsampled while wet to retain the AVS portion. Solvent extractable sulfur (i.e., elemental S) occasionally produced enough yield to measure the $\delta^{34}S$ composition, whereas the acid-volatile sulfide yield was always minimal and too low to measure the $\delta^{34}S$ composition (data not shown). The isotopic composition of CRS in sequentially extracted sediments (i.e., pyrite only) on average is indistinguishable within 1σ from the CRS of bulk sediments (integrating pyrite, elemental S, and monosulfides) (Table 2). The bulk sediment CRS ranges from −1.9 to −11.2‰ and the pyrite fraction (following sequential extraction) ranges from −4.4 to −10.8‰ (Table 2). Sedimentary pyrite $\delta^{34}S_{py}$ values were highest (−5.6 ± 1.0‰) in the transition zone sediments and lowest in sediments underlying seagrass stands (−8.1 ± 1.7‰) (Table 2). However, all sedimentary pyrite was isotopically depleted in ^{34}S relative to the hydrothermal vent fluid ($\delta^{34}S_{H2S} = +2.7 \pm 0.6$‰). The only samples with statistically significant deviations between these bulk sediment and pyrite-only CRS fractions were found at depth (> 11 cm) near the vent source and in the transition zone (shaded in Table 2). These samples were targeted specifically to analyze the DCM extractable sulfur isotopic composition (i.e., elemental sulfur), which was relatively consistent with an average $\delta^{34}S_{ES}$ of −0.5 ± 2.7‰ ($n = 7$) and slightly lower than the endmember $\delta^{34}S$ composition of hydrothermal sulfide.

3.3. Diversity and distribution of sulfur-metabolizing microorganisms

Sequences of 16S rRNA genes from extracted environmental DNA were analyzed to identify the dominant microorganisms with the potential to mediate biogeochemical transformations. The data show that the fraction of OTUs (operational taxonomic units) attributed to putative sulfur-utilizing microbes is elevated in hydrothermally influenced
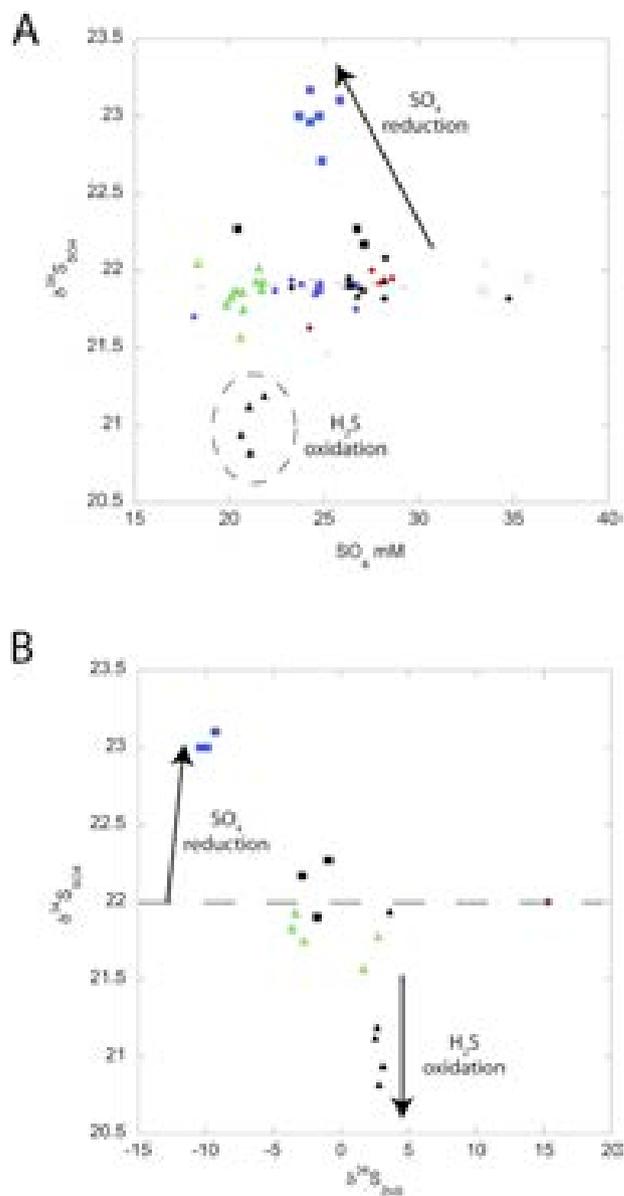
Fig. 3. (A) Sulfur chemistry of porewaters are compared between locations (vent: triangles, transition zone: squares, seagrass stands: diamonds, background sediments: dashes, background seawater: open circles, vent gas: crosses) and between different sampling days (5/21: red, 5/22: blue, 5/23: green, 5/24: black). (B) A subset of porewater samples contained concentrations of both sulfate and sulfide that allowed for parallel isotopic measurements. (For interpretation of the references to colour in this figure legend, the reader is referred to the web version of this article.)

sediments near the vent source and in the transition zone relative to seawater (Fig. 5a). Porewater fluids (taken at 10 cm depth) from the vent source and the transition zone have very similar relative abundances of putative sulfur oxidizers and sulfur reducers (Fig. 5a, red outline), even when divided into subcategories based on specific inferred metabolic pathways (Fig. 5b). DNA sequences from sediments beneath seagrass stands and in distal background sediments show proportionally more putative sulfide oxidizers at the surface and an increase toward more sulfur reducers at depth (Fig. 5b). Sediments near the vent source and in the transition zone do not show a strong trend with depth (Fig. 5b), although the relative fraction of sulfur oxidizers was much higher than reducers in the transition zone sediments compared to vent sediments and all other sites (Fig. 5a).
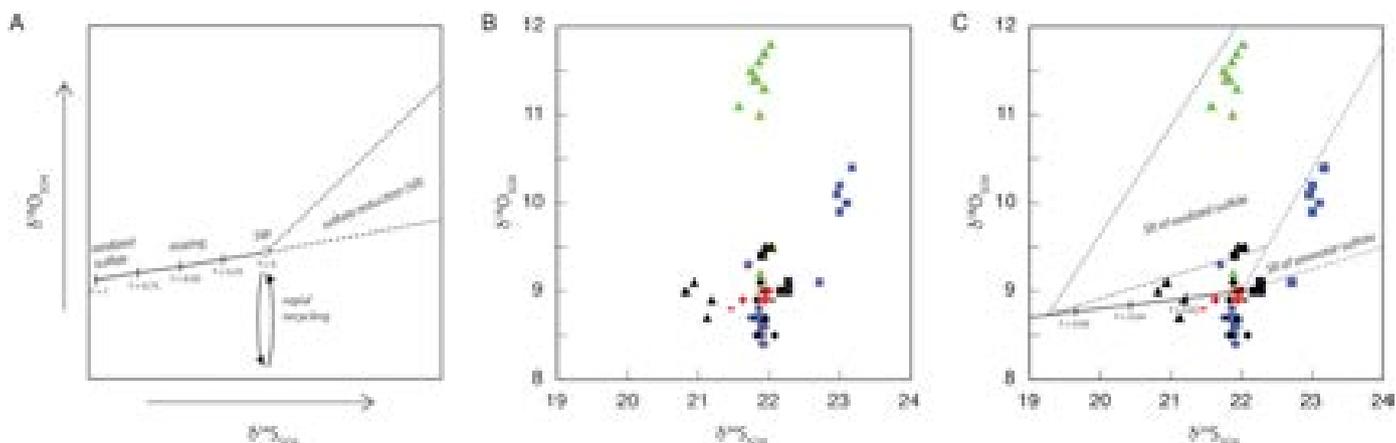
Fig. 4. (A) The processes of mixing between oxidized sulfide and seawater sulfate (SW), sulfate reduction (SR), or rapid cycles of oxidation and reduction can influence the $\delta^{34}S$ and $\delta^{18}O$ of sulfate within the porewaters. (B) The paired isotope compositions of Milos porewaters (vent: triangles, transition zone: squares, seagrass stands: diamonds, background sediments: dashes, background seawater: open circles, vent gas: crosses) collected on different days (5/21: red, 5/22: blue, 5/23: green, 5/24: black) can be explained by (C) the sulfate reduction of primary seawater sulfate (SR of seawater sulfate), sulfide oxidation, and subsequent reduction of secondary sulfate (SR of oxidized sulfide). (For interpretation of the references to colour in this figure legend, the reader is referred to the web version of this article.)

3.4. Sulfide films

Sulfide films were deployed over 5 successive days. By capturing sulfide over several (e.g., 4–16) hours, these films sample timescales intermediate between those represented by in-situ voltammetry or porewater extractions (short) and sedimentary minerals (long). Replicate films were deployed back to back within sediments to investigate spatial variability (e.g., caused by horizontal advection of fluids). The variability between replicate films, < 1‰, is much smaller than that observed between different sampling days (Fig. 6, open vs. closed symbols). The films provide more spatially continuous, time-integrated monitoring of sulfur cycling in the surface sediments that complement the temporally and spatially sparser observations from porewaters. Based on previous work, films exposed to similar concentrations (< 1.5 mM H_2S) continuously capture sulfide without saturating for 20 h, although the rate of capture decreases after ~4 h (Fike et al., 2017). Therefore, although longer exposure times allow greater accumulation of sulfide on film, the cumulative $\delta^{34}S$ signal captured will disproportionately reflect the first few hours of exposure in sediments. Films placed in sediments near the vent source (Fig. 6, squares, diamonds) captured both hydrothermal and microbially influenced endmember $\delta^{34}S$ values on different days during daytime (4–6 h) sampling periods. One overnight (16 h) deployment at the vent-transition boundary captured intermediate $\delta^{34}S_{H2S}$ with no gradient with depth (Fig. 6, circles). During that same deployment period, film placed in the center of the transition zone captured a gradient in $\delta^{34}S_{H2S}$ between the endmember values (Fig. 6, triangles). The results from films reproduced the observed range of $\delta^{34}S_{H2S}$ values (~ −10 to +2‰) measured in porewaters, notably without expanding this range. For example, porewater sulfide on the days sampled in this study group into three distinct clusters of $\delta^{34}S$ values (Fig. 6, grey zones) with: 1) the lowest $\delta^{34}S$ values (−9.8 ± 0.5‰, n = 3) in transition zone porewaters, 2) $\delta^{34}S$ values identical to the hydrothermal endmember (+2.6 ± 0.5‰, n = 5) nearest the vent source, and 3) intermediate $\delta^{34}S$ values (−2.3 ± 1.1‰, n = 7) found in both the vent source and the transition zone. For reference, the elemental sulfur from both the vent source and transition zone (Fig. 6, yellow zone) were most similar to the vent endmember porewater cluster, while the $\delta^{34}S$ of pyrite (Fig. 6, green zone) resembles only the cluster of porewater sulfides with relatively low $\delta^{34}S$ values.

3.5. Microelectrode measurements

In-situ measurements of porewater chemistry using potentiometric microelectrodes provide second- to minute-scale temporal resolution of electrochemically active species (Luther et al., 2008). Deployment of electrodes at both 2 cm and 5 cm depths in sediments across the transect from the vent source, through the transition zone, to the seagrass area

Table 1
Sulfur yield of CRS extracted from bulk sediments and after sequential extraction removing DCM-soluble sulfur and AVS. Both values reported in mmol S/g wet sediment. Depth horizons not available are indicated by n.a. Samples for which duplicate measurements were averaged are indicated with *.

Depth (cm)	Vent		Transition		Seagrass		Background	
	Pyrite fraction	Bulk CRS	Pyrite fraction	Bulk CRS	Pyrite fraction	Bulk CRS	Pyrite fraction	Bulk CRS
1	22.1	70.0	21.3	27.5	6.4	19.7	2.7*	5.5
3	24.4	64.6	39.2	18.9	11.4	37.7	2.8*	4.2
5	41.2	73.3	32.8	43.1	3.3	37.8	2.1*	3.9
7	21.7	28.2	29.3	52.5	7.1	39.6	1.3*	2.3
9	13.6	54.2	31.4	56.1	13.2	37.3	3.0*	2.6
11	18.8	37.7	23.8	38.8	12.1	44.2	2.7*	4.0
13	18.6	61.3	18.0	83.9	n.a.	n.a.	4.5*	5.2
15	50.1*	51.5	23.5	50.0	n.a.	n.a.	2.6*	9.3
17	54.2*	53.5	21.1	88.4	n.a.	n.a.	n.a.	n.a.
19	23.6	29.9	42.4	92.0	n.a.	n.a.	n.a.	n.a.
21	61.1	71.6	n.a.	n.a.	n.a.	n.a.	n.a.	n.a.

Table 2

Isotopic compositions (‰, V-CDT) of CRS extracted from bulk sediments and after sequential extraction removing DCM-soluble sulfur and AVS. Depth horizons not available are indicated by n.a. Grey shading indicates samples with significant deviation between the $\delta^{34}S$ of the pyrite fraction from the bulk CRS.

| Depth (cm)	Vent		Transition		Seagrass		Background	
	Pyrite fraction	Bulk CRS	Pyrite fraction	Bulk CRS	Pyrite fraction	Bulk CRS	Pyrite fraction	Bulk CRS
1	-5.8	-5.2	-5.2	-5.3	-5.9	-4.9	-8.6	-8.1
3	-7.8	-7.2	-4.4	-4.6	-6.7	-5.9	-7.7	-8.1
5	-10.8	-11.2	-6.7	-6.7	-7.2	-7.1	-8.3	-7.7
7	-7.9	-8.7	-7.3	-7.2	-10.2	-6.4	-8.0	-6.6
9	-6.8	-6.6	-6.3	-6.8	-8.7	-9.4	-7.5	-5.7
11	**-7.1**	-5.0	-4.8	-4.3	-9.7	-10.2	-4.9	-5.2
13	**-7.5**	-5.6	**-6.2**	-3.3	n.a.	n.a.	-5.1	-5.4
15	**-7.6**	-5.1	**-5.0**	-4.5	n.a.	n.a.	-5.2	-5.6
17	-5.3	-4.7	**-4.4**	-1.9	n.a.	n.a.	n.a.	n.a.
19	**-7.2**	-5.8	**-5.5**	-2.7	n.a.	n.a.	n.a.	n.a.
21	-8.3	-8.4	n.a.	n.a.	n.a.	n.a.	n.a.	n.a.
Average	**-7.5**	**-6.7**	**-5.6**	**-4.7**	**-8.1**	**-7.3**	**-7.0**	**-6.6**
1σ	**1.4**	**2.0**	**1.0**	**1.8**	**1.7**	**2.1**	**1.7**	**1.3**
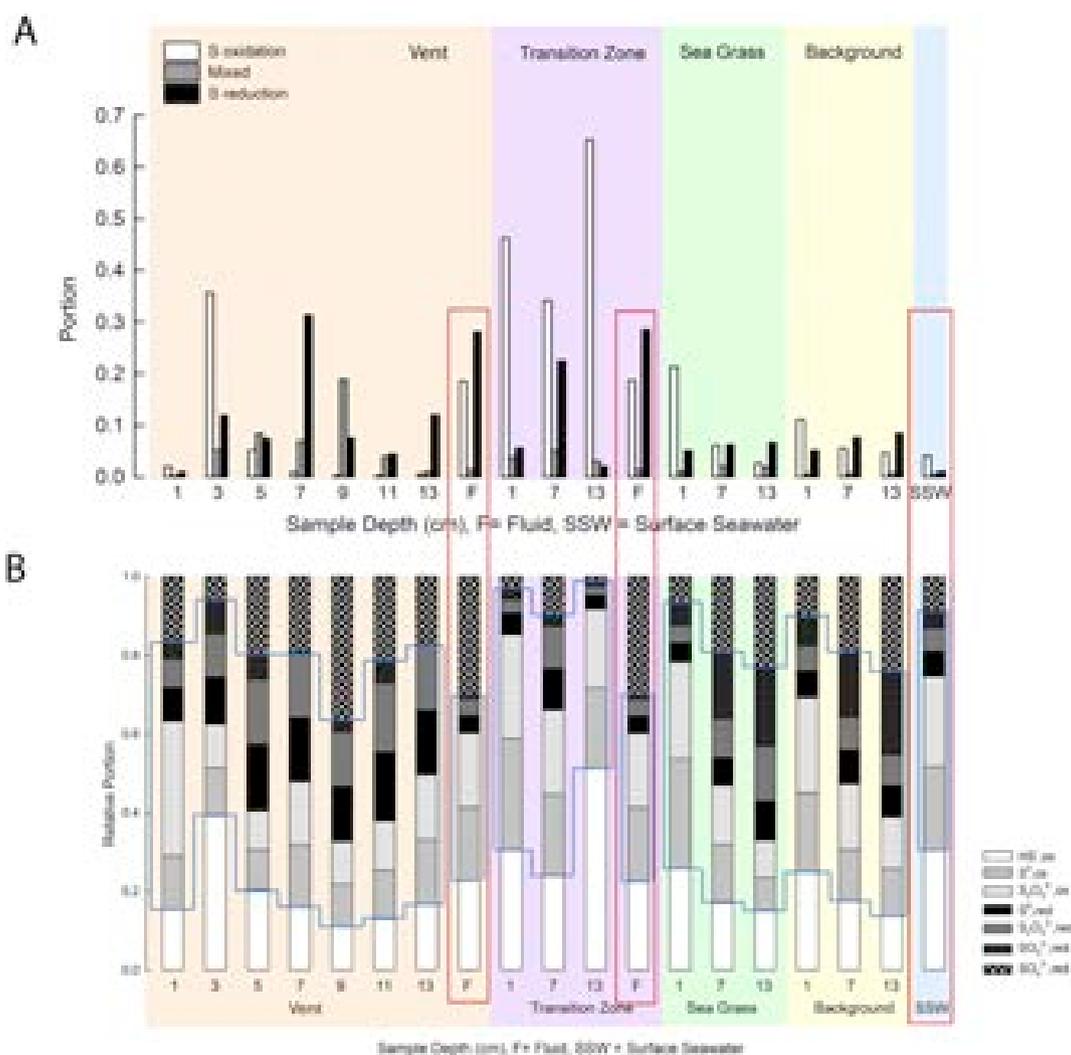
Fig. 5. (A) Relative portion of total sequences attributed to sulfur metabolisms based on BLAST results of 16S rDNA sequences. The relative balance of sulfur oxidizers to reducers in sediment microbial communities beneath the vent and transition zones are very different from the overlying water column (boxed in red). (B) A more detailed evaluation of the sulfur-utilizing portion of the community reveals a relatively high proportion of microorganisms known to utilize intermediate redox states of sulfur (boxed in blue). (For interpretation of the references to colour in this figure legend, the reader is referred to the web version of this article.)

reveals temporal variability in sulfide speciation (Fig. 7). In particular, the variability in sulfide and polysulfide abundance with time near the vent source was much greater than in the transition zone. Sulfide concentrations remained high (300–600 μM) throughout this time period in the transition zone (Fig. 7). A weak but fairly constant signal corresponding to elemental sulfur (S_8) was detected at depth beneath the seagrass stand (Fig. 7).
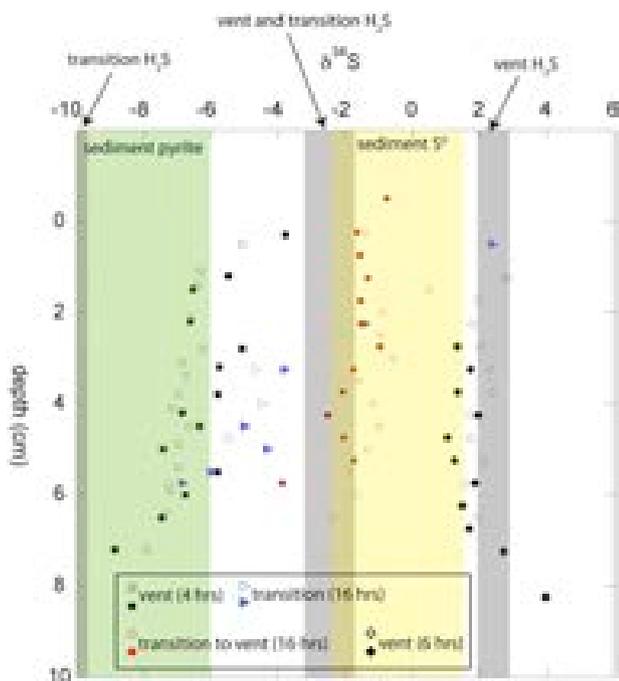
Fig. 6. The δ^{34}S of sulfide captured on films from different days (replicate films indicated with open vs. solid symbols) varies between the endmember compositions observed in porewaters. Sulfide abundance captured on the films enabled analysis only in sediments near the vent source (squares, diamonds) and in the transition zone (triangles, circles). The isotopic composition of porewater sulfide extracted from the cores clustered into three regions indicated by grey shading: a depleted cluster (transition H_2S), a hydrothermal cluster (vent H_2S), and an intermediate cluster (vent and transition H_2S). For comparison, the range in $\delta^{34}S_{pyrite}$ (green shading) and in elemental sulfur (yellow shading) is also shown. (For interpretation of the references to colour in this figure legend, the reader is referred to the web version of this article.)
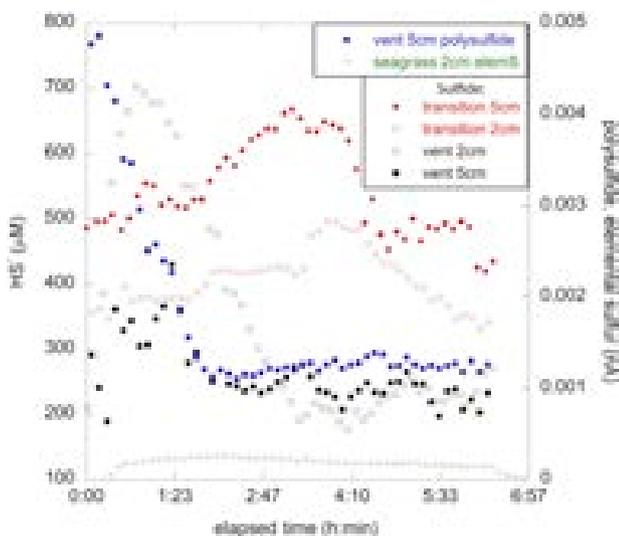

Fig. 7. Electrochemical measurements of reactive sulfur species (sulfide, polysulfide and elemental sulfur) monitored every 10 min at both 2 cm and 5 cm sediment depths along the transect from vent source to the peripheral seagrass stand reveal highly variable subsurface sulfide concentrations over a 7-h time period.

4. Discussion

The use of multiple measurements over a range of time periods aids in interpreting the field observations by integrating across the

timescales intrinsic to each (Fig. 2). Our combined approach of studying the in-situ porewater chemistry, 16 s rDNA sequences, and composition of sulfur minerals reveals the highly dynamic sulfur cycle of a shallow sea hydrothermal vent, where biogeochemical signatures indicate microbial sulfate reduction, sulfide oxidation, and rapid recycling of sulfur intermediates that vary with location and time.

4.1. Isotopic evidence for microbial sulfate reduction and sulfide oxidation

Intracellular enzymatic reactions within sulfate-reducing microorganisms produce kinetic isotope effects (Kaplan and Rittenberg, 1964; Canfield, 2001; Wing and Halevy, 2014), resulting in residual sulfate enriched in ^{34}S and product sulfide depleted in ^{34}S. The full extent of isotopic fractionation between sulfate and sulfide can depend upon sulfate availability, rates of reduction, microbial community, and temperature (Sim et al., 2011; Leavitt et al., 2013; Bradley et al., 2011; Johnston et al., 2007); fractionation is generally highest ($\Delta^{34}S_{H2S-SO4}$ up to 70‰) at low rates of cell-specific sulfate reduction and decreases at higher rates (Sim et al., 2011; Wing and Halevy, 2014). Oxygen isotopes within the sulfate molecule also undergo enzymatically controlled kinetic fractionation. However, back-reactions during sulfate reduction promote oxygen isotope exchange between intracellular sulfur intermediates (e.g., SO_3^{2-}) and ambient water molecules (Brunner and Bernasconi, 2005; Brunner et al., 2005). The trends observed in the paired increases in $\delta^{18}O_{SO4}$ and $\delta^{34}S_{SO4}$ can be driven by variable rates of multiple enzymatic steps within the cells of sulfate-reducing microorganisms (Mizutani and Rafter, 1969; Bottcher et al., 1998; Brunner et al., 2005, 2012; Antler et al., 2013; Turchyn et al., 2010). The upper and lower ranges of these reactions can be constrained with Rayleigh equations (Antler et al., 2013; Turchyn et al., 2010; Gilhooly et al., 2016) that account for kinetic and equilibrium isotope fractionations that occur during sulfate reduction (Fig. 4a, arrays defining "sulfate reduction (SR)" field). Extracellular oxidation reactions (e.g. Aller et al., 2010) can also produce patterns of wide variation in $\delta^{18}O_{SO4}$ with little change in $\delta^{34}S_{SO4}$ relative to ambient seawater sulfate (Fig. 4a, "rapid cycling").

Clear evidence of microbial sulfate reduction was observed in the transition zone, with porewater sulfide of low $\delta^{34}S_{H2S}$ (i.e., $\delta^{34}S_{H2S} < < \delta^{34}S_{hydrothermal}$). Moreover, porewater sulfates collected on May 22 exhibit a clear increase in $\delta^{34}S_{SO4}$ as sulfate concentrations decrease (Fig. 3a). Here, $\delta^{34}S_{SO4}$ increases due to progressive sulfate reduction, while $\delta^{34}S_{H2S}$ values decrease with depth due to diminished contributions from hydrothermal sources (Fig. 3b). Comparing $\delta^{34}S_{SO4}$ and $\delta^{18}O_{SO4}$ of residual sulfate provides additional evidence supporting microbial sulfate reduction within transition zone sediments. Porewaters from transition zone samples plot within the range expected for microbial reduction of seawater sulfate (Fig. 4c). In addition, OTUs associated with potential sulfate reducers were present, although not dominant, at all depths in the transition zone (Fig. 5).

Sulfide oxidation was apparent in the porewaters sampled nearest the vent source on certain days based on parallel decreases in $\delta^{34}S_{SO4}$ and $\delta^{18}O_{SO4}$ below those of ambient seawater. When considering the sulfur isotopic composition of coeval sulfate and sulfide, the decrease in $\delta^{34}S_{SO4}$ values of vent samples collected on May 24 relative to seawater suggest a contribution of partial H_2S oxidation to the sulfate pool (Fig. 3b); however, there is no such evidence within the $\delta^{34}S_{SO4}$ of vent samples collected on May 23 (Fig. 3b). The $\delta^{18}O_{SO4}$ values provide added insight and suggest variable activity of sulfate reducers on the days these vents were sampled (Fig. 4c). The May 24 vent data plot along a mixing line (Fig. 4a, 'mixing') between Palaeochori Bay seawater sulfate ($\delta^{34}S_{SO4}$ = 22‰, $\delta^{18}O_{SO4}$ = 9‰) and secondary sulfate produced from oxidation of hydrothermal sulfide by Milos seawater ($\delta^{34}S_{H2S}$ = 2.5‰, $\delta^{18}O$ = 1.1‰, see Methods). The sulfur isotopic composition of May 24 vent porewater sulfate can be explained by an admixture of 2–3% oxidized sulfide into the ambient sulfate pool (Fig. 4c, f = 0.02 to 0.03) with no additional microbial sulfate

reduction. A similar proportion of sulfide oxidation was observed in a previous study of hydrothermal circulation in Palaeochori Bay (Gilhooly et al., 2014). Curiously, vent porewaters sampled May 23 exhibit different isotope patterns. The $\delta^{34}S_{SO4}$ values tend to be slightly lower than seawater sulfate; however, $\delta^{18}O_{SO4}$ values are approximately 2‰ higher than seawater sulfate (Fig. 4b). Oxygen isotope exchange between sulfate-oxygen and ocean water at the higher temperatures ($> 40\,°C$) and low pH (< 5) of these porewaters would produce $\delta^{18}O_{SO4}$ values that are lower than seawater sulfate (Aller et al., 2010; Chiba and Sakai, 1985; Lloyd, 1968) and therefore cannot explain the observed values. Rather, these high $\delta^{18}O_{SO4}$ values are consistent with sulfate reduction of a mixed fluid that contains background seawater and oxidized sulfide (Fig. 4c, 'SR of oxidized sulfide').

The patterns revealed in the paired sulfur and oxygen isotope compositions of porewater sulfate provide additional detail not readily apparent in the analysis of $\delta^{34}S_{SO4}$ alone. For instance, the surficial sediments (upper 5 cm) of the transition zone sediments have $\delta^{18}O_{SO4}$ values that are ~ 1‰ lower than seawater. Porewater sulfates within seagrass beds and background sediments are also depleted in ^{18}O without significant changes in sulfur isotope composition relative to seawater sulfate. *Re*-oxidation during abiotic or biotic reactions can effectively drive $\delta^{18}O_{SO4}$ values lower than those of seawater sulfate with no net change in $\delta^{34}S_{SO4}$ (Aller et al., 2010). The 16S rDNA data further suggest these sites may have an active oxidative microbial sulfur cycle (Fig. 5). OTUs associated with potential sulfide oxidizers represent the larger fraction of total diversity in the transition zone as well as the surficial sediments within seagrass and background sites (Fig. 5). Sulfide concentrations are low beneath seagrass stands and in background sediments in the top 20 cm (Fig. S1b), suggesting the sulfidic zone is much deeper in these regions. Daytime photosynthesis within seagrass meadows likely pumps oxygen into the sediments (Jensen et al., 2005; Glud, 2008) and oxidants may be replenished in the surficial background sediments by tidal action (Yucel et al., 2013). Both of these processes could result in rapid redox cycling in these regions.

4.2. How reliably do proxies record temporal variability?

The paired sulfur and oxygen isotope compositions of porewater sulfate appear to be responsive to the relative influences of sulfur oxidation and reduction pathways within each site. Although the chemical data are broadly consistent with the genetic diversity and metabolic potential of the sediments, porewater within sediments reflect averaged geochemical processes and microbial activity on the scale of hours (Fig. 2). Thus, sampling pore fluids from sediments cored on multiple days will capture some of the range in sulfur cycling within these highly dynamic systems. However, real-time in-situ measurements of sulfur speciation (Fig. 7) and the $\delta^{34}S_{H2S}$ of dissolved sulfide (Fig. 6) indicate an instantaneous chemical and isotope composition that can be widely different from those measured in porewater extractions (Fig. 3) or in sedimentary sulfides (Fig. 8). The film results emphasize the transience over time and space of sulfur cycling in these sediments; this is in contrast to the idea of a fixed transition from hydrothermal sulfide to microbial sulfide sources with increasing distance away from the venting area, as suggested by the porewaters. Tracking the shifting porewater $\delta^{34}S_{H2S}$ over consecutive days compared to pyrite $\delta^{34}S_{py}$ highlights the temporal variability in this dynamic system and the necessity of collecting a timeseries of samples in order to more fully characterize the geochemistry of the system in a temporal manner (Fig. 8). The agreement between independent isotopic assays ($\delta^{34}S_{H2S} = -9$ to $+4$‰) suggests that the full range of aqueous $\delta^{34}S_{H2S}$ present in this setting was captured, at least at the time of this sampling. However, the range in $\delta^{34}S_{py}$ is much smaller (-10.8 to -4.4‰; Table 2) with no spatial patterns along the transect and, notably, no values close to hydrothermal sulfide ($\delta^{34}S_{H2S} = +2.5$‰) nor more depleted values (e.g., -25‰ to -45‰) typical of biological sulfate

reduction in many marine systems (Canfield et al. 2001; Fike et al., 2015).

Hour-scale temporal variability of concentrations at depth in the sediments (Fig. 7) was greatest nearest the vent (i.e., the zone likely to be most heavily impacted by advection). Geochemical variability derives from a combination of possible processes, including: the flux of sulfide to a particular point, the consumption (via a number of (a)biotic processes) of that sulfide over time, and the mixing of sulfidic fluids with oxic or suboxic water. Hydrodynamic variability couples to the geochemical variability and can be represented as chaotic fluctuations in advective pathways, changes in diffusive flux through changing boundary layer conditions, as well as variable advection of more oxygenated surface water associated with wave height and sand ripple migration in near-shore permeable sediments (Falter and Sansone, 2000; Fram et al., 2014; Yücel et al., 2013). This variation in geochemical regimes perhaps explains the large fraction of sulfur-utilizing microbes in all the sediments sampled that can either oxidize or reduce a range of sulfur phases of intermediate oxidation state (Fig. 5b, blue outline). This suggests a degree of metabolic flexibility is maintained within the microbial community inherent in all the sediments in the region, which would be an advantage in an unstable advection-dominated environment. DNA can be stable within sedimentary environments for days to years, and recovery of 16S rDNA genes will include both active and dormant cells (Dick and Lam, 2015). Therefore, although the microbial biomass in sediments throughout the Saganaki vent field has the metabolic potential for both microbial sulfate reduction and sulfide oxidation, the expression of microbial sulfate reduction and sulfide oxidation is transient over time and space. These combined observations highlight the need for caution when making interpretations about microbial functions based on field data that might not represent signals averaged over the timescales most relevant to the ambient microbial communities.

4.3. A biased record from sedimentary minerals?

Sulfur minerals in marine sediments accumulate on the order of years to thousands of years (Fig. 2). Thermodynamically stable minerals (e.g., pyrite) can ultimately be preserved in the rock record, where they are often used to reconstruct and interpret sulfur cycling in Earth's history (Strauss, 1999; Canfield, 2004; Hurtgen et al., 2005; Fike et al., 2006; Fike and Grotzinger, 2008; Fike and Grotzinger, 2010; Gill et al., 2011; Jones and Fike, 2013; Fike et al., 2015). Therefore, it is essential to understand the relative contributions to the bulk sediment Fe-sulfide (e.g., pyrite) record of both microbial and abiotic reactions and the time scales that each may represent. As the isotopic compositions indicate, porewater samples represent a mixture of two endmember (hydrothermal and biological) sources of sulfide overprinted by complex sulfur redox cycling, such that the true microbial endmember is unknown. In addition, these sediments are deposited in relatively shallow water (~12 m) in a dynamic, high-energy environment characterized by frequent sediment remobilization during storms. One such storm occurred during prior sampling (Gilhooly et al., 2014) and resulted in the overnight disappearance of the ubiquitous hydrothermal precipitates at the sediment-water interface surrounding venting regions. We suggest that frequent physical mixing results in a nearly uniform distribution of biogenic and hydrothermal Fe-sulfides throughout the region, as seen in the relative constancy of the sedimentary pyrite record across the transect (Fig. 8).

The isotopic fractionation between ambient sulfate and Fe-sulfides ($\varepsilon \sim 30$‰) that is observed here is much less than typical for many marine sediments (e.g., Canfield, 2001) and slightly less than half of the maximum known for sulfide produced by sulfate reducers (Sim et al., 2011; Leavitt et al., 2013; Wing and Halevy, 2014). Combined with the low organic content of these coarse-grained, quartz-rich sandy sediments (Gilhooly et al., 2014), analysis of the sedimentary record alone would suggest a shallow marine depositional environment with a
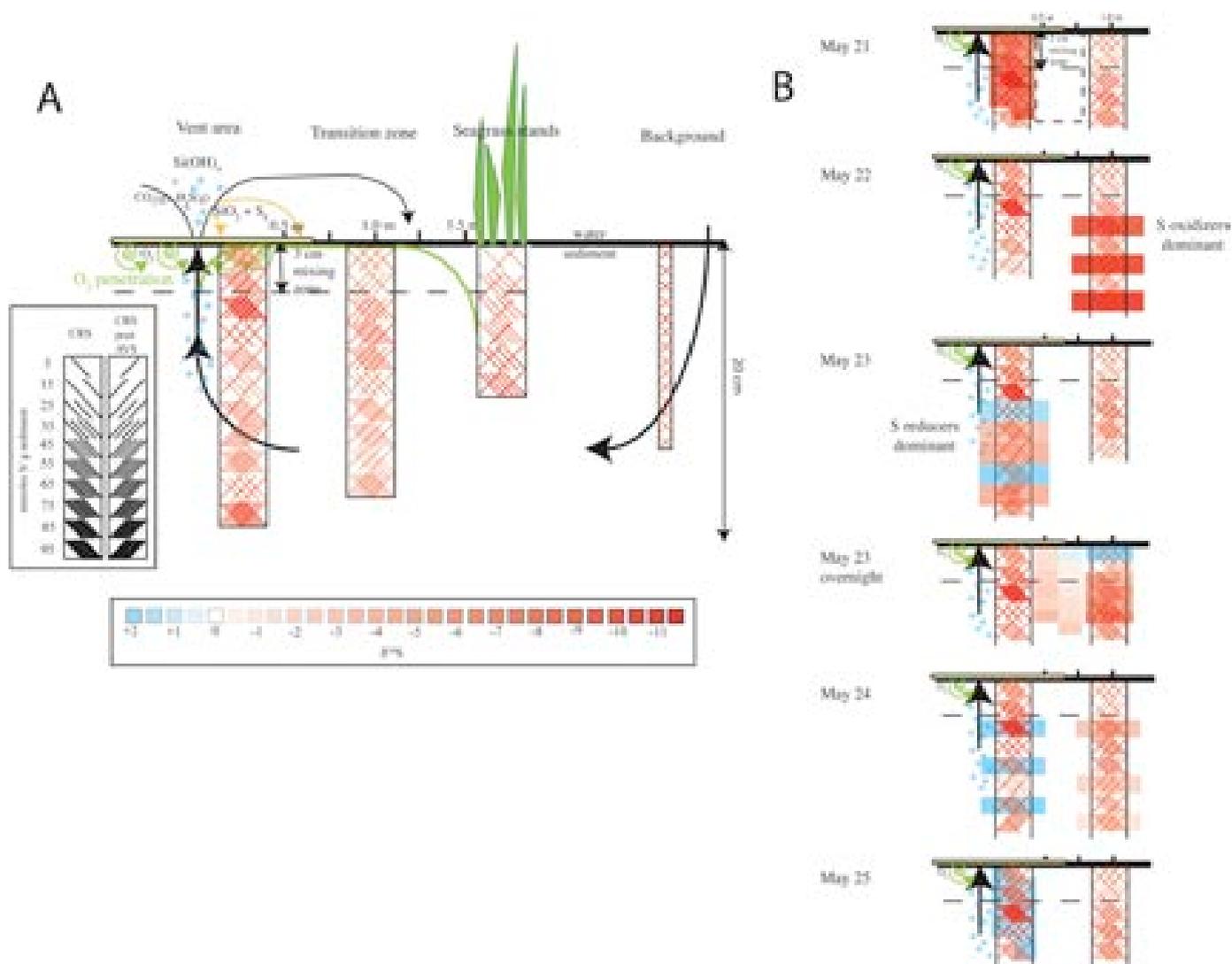
Fig. 8. (A) Schematic in cross-section of the Saganaki vent field with abundance (number of hatch marks) and $\delta^{34}S$ (colour) of sediment bulk CRS extractions displayed with hatch marks and hydrothermal flow indicated by arrows. (B) The time series of sulfide film deployments in the vent and transition areas (shown as solid colors representing $\delta^{34}S$) over several days reveals a gradual transition from microbially produced sulfide to hydrothermal (abiotic) sulfide between May 21 and May 25. For the dates corresponding to sediment collection for PCR analysis, the dominant sulfur metabolizing group is indicated beside the cross section.
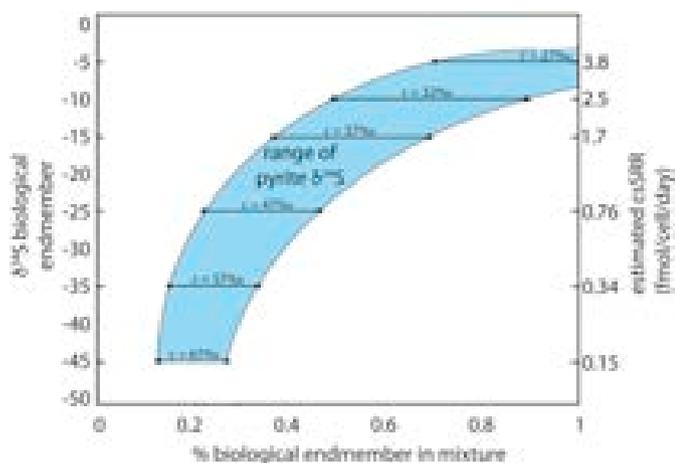

Fig. 9. Schematic showing the estimated range in isotopic composition of endmember microbial sulfide required at various mixing ratios with hydrothermal sulfide that would result in the range of pyrite $\delta^{34}S$ observed in this study. Cell-specific sulfate reduction rates (csSRR) are estimated using an empirical fit to experimental results from Sim et al., 2011.

perplexing apparent fractionation consistent with moderately fast rates of sulfate reduction or closed system Rayleigh distillation. The presence of hydrothermal activity is not readily apparent from just the sedimentary record due to the frequent physical mixing in the system. Even using multiple analytical techniques in this study, we cannot conclusively determine the $\delta^{34}S_{H2S}$ of the microbial endmember or the relative abundance of the respective endmembers. Two possible endmember scenarios could explain these observations: either (1) the expressed microbial fractionation in these settings is the observed ~30‰ and the sulfide from which Fe-sulfides formed contains a high fraction of microbial sulfide, or (2) microbial fractionation is larger (up to the theoretical maximum of 70‰) and Fe-sulfides formed from corresponding higher proportions of hydrothermal sulfide. In the first scenario, a fractionation of 30‰ is lower than what might be expected from the low organic carbon loading of these sediments. Specifically, such a low fractionation would seem to require an additional (abundant) electron donor. Given the hydrothermal context investigated here, this could be provided by dissolved organics (e.g., formate, acetate) sourced within the hydrothermal system – or from dissolved hydrogen from within these fluids. The latter has been measured as an abundant constituent of vent gas from Paleochori Bay (up to 9%; Dando

et al., 1998). Such hydrothermal stimulation of microbial sulfate reduction could be consistent with the increase in pyrite content proximal to the vent locations. A simple mixing calculation between endmember hydrothermal sulfide ($\delta^{34}S_{H2S} = +2.5‰$) and a microbial endmember assuming different fractionations can constrain the fraction of microbial input required to produce the range of $\delta^{34}S_{py}$ observed (Fig. 9). In the first case, a fractionation of ~30‰ would mean 50–90% of the sulfide in pyrite was derived from a microbial source, consistent with faster rates of sulfate reduction. In this case, the sedimentary TOC and $\delta^{34}S_{py}$ records would appear inconsistent in the absence of porewater data (e.g., in the rock record) – in large part because the fast rates of sulfate reduction would be driven by dissolved hydrothermal components (e.g., H_2 or dissolved organics like formate or acetate) that do not necessarily leave a readily apparent record in sediments. In the second case, microbial sulfate reduction rates would be slow and the biological $\delta^{34}S_{H2S}$ endmember could approach $-45‰$ (Wing and Halevy, 2014), consistent with the low organic content of these sediments (Gilhooly et al., 2014). In this case, the microbial endmember would only contribute 10–30% of the sulfide in Fe-sulfides and the presence of microbial sulfate reduction would be swamped out by hydrothermal input, which itself might not be obvious from just the sedimentary record. Isotopic analyses of individual pyrites (e.g., Fischer et al., 2014; Gomes et al., 2017) could help resolve the origin of the sulfide in these pyrites. The second scenario would be expected to produce a distinct bimodal $\delta^{34}S_{py}$ distribution with peaks centered around both hydrothermal ($+2.5‰$) and biogenic ($-45‰$) endmembers, whereas the former would be expected to yield a more unimodal distribution centered around $-10‰$.

5. Conclusions

In this study, an interdisciplinary combination of biogeochemical proxies was used to investigate the contributions of ephemeral microbial activity to sulfur cycling in dynamic hydrothermal environments. The suite of results over several days of sampling reveal a coherent - yet ephemeral - microbial sulfur cycle. The inconsistency between the spatial patterns in the 16S rDNA and porewater chemistry suggests that much of the complex suite of environmental (advection of hydrothermal fluids) and biological (both sulfate reduction and sulfide oxidation) processes that are occurring here are not necessarily well reflected in the isotopic signatures in porewaters. In addition, the discrepancy between the instantaneous porewater $\delta^{34}S_{H2S}$ and the $\delta^{34}S_{py}$ of geologically stable sulfur mineral phases within the sediments, likely due to sedimentary remobilization during storms (Aller et al., 2010), creates an apparent signature that masks both the biotic and abiotic endmember processes at work in this system. These inconsistencies partly reflect how fast microbial populations respond to changing chemical conditions, and the relative speed of mineral formation and chemical exchange in response to dynamic porewater chemistry. These results suggest the potential for biosignature preservation in these types of settings may rest in understanding the impacts of dynamic, ephemeral, chaotic porewater chemistry on microbial populations and physiology as well as on mineral formation and isotopic exchange.

Supplementary data to this article can be found online at https://doi.org/10.1016/j.marchem.2018.11.002.

Acknowledgements

References

Akerman, N.H., Price, R.E., Pichler, T., Amend, J.P., 2011. Energy sources for chemolithotrophs in an arsenic- and iron-rich shallow-sea hydrothermal system. Geobiology 9, 436–445.

Aller, R.C., Madrid, V., Chistoserdov, A., Aller, J.Y., Heilbrun, C., 2010. Unsteady diagenetic processes and sulfur biogeochemistry in tropical deltaic muds: Implications for oceanic isotope cycles and the sedimentary record. Geochim. Cosmochim. Acta 74, 4671–4692.

Antler, G., Turchyn, A.V., Rennie, V., Herut, B., Sivan, O., 2013. Coupled sulfur and oxygen isotope insight into bacterial sulfate reduction in the natural environment. Geochim. Cosmochim. Acta 118, 98–117.

Balci, N., Shanks III, W.C., Mayer, B., Mandernack, K.W., 2007. Oxygen and sulfur isotope systematics of sulfate produced by bacterial and abiotic oxidation of pyrite. Geochim. Cosmochim. Acta 71, 3796–3811.

Bottcher, M.E., Brumsack, H-J., de Lange, G.J., 1998. Sulfate reduction and related stable isotope (^{34}S, ^{18}O) variations in interstitial waters from the eastern Mediterranean, in: Robertson, A.H.F., Richter, K.-C., Camerlenghi, A.(Eds.), Proceedings of the Ocean Drilling Program, Scientific Results. vol. 160, 365–373.

Bradley, A.S., Leavitt, W.D., Johnston, D.T., 2011. Revisiting the dissimilatory sulfate reduction pathway. Geobiology 9, 446–457.

Brendel, P.J., Luther, G.W.I., 1995. Development of a gold amalgam voltammetric microelectrode for the determination of dissolved Fe, Mn, O_2, and S (-II) in porewaters of marine and freshwater sediments. Environ. Sci. Technol. 29, 751–761.

Brunner, B., Bernasconi, S.M., 2005. A revised isotope fractionation model for dissimilatory sulfate reduction in sulfate reducing bacteria. Geochim. Cosmochim. Acta 69, 4759–4771.

Brunner, B., Bernasconi, S.M., Kleikemper, J., Schroth, M.H., 2005. A model for oxygen and sulfur isotope fractionation in sulfate during bacterial sulfate reduction processes. Geochim. Cosmochim. Acta 69, 4773–4785.

Brunner, B., Einsiedl, F., Arnold, G.L., Muller, I., Templer, S., Bernasconi, S.M., 2012. The reversibility of dissimilatory sulphate reduction and the cell-internal multi-step reduction of sulphite to sulphide: insights from the oxygen isotope composition of sulphate. Isot. Environ. Health Stud. 48, 33–54.

Canfield, D.E., 2001. Isotope fractionation by natural populations of sulfate-reducing bacteria. Geochim. Cosmochim. Acta 65, 1117–1124.

Canfield, D.E., 2004. The evolution of the Earth surface sulfur reservoir. Am. J. Sci. 304, 839–861.

Canfield, D.E., Raiswell, R., Westrich, J.T., Reaves, C.M., Berner, R.A., 1986. The use of chromium reduction in the analysis of reduced inorganic sulfur in sediments and shales. Chem. Geol. 54, 149–155.

Caporaso, J. Gregory, Kuczynski, Justin, Stombaugh, Jesse, Bittinger, Kyle, Bushman, Frederic D., Costello, Elizabeth K., Fierer, Noah, et al., 2010. QIIME allows analysis of high-throughput community sequencing data. Nat. Methods 7 (5), 335.

Caporaso, J. Gregory, Lauber, Christian L., Walters, William A., Berg-Lyons, Donna, Lozupone, Catherine A., Turnbaugh, Peter J., Fierer, Noah, Knight, Rob, 2011. Global patterns of 16S rRNA diversity at a depth of millions of sequences per sample. Proc. Natl. Acad. Sci. 108 (Supplement 1), 4516–4522.

Chiba, H., Sakai, H., 1985. Oxygen isotope exchange rate between dissolved sulfate and water at hydrothermal temperatures. Geochim. Cosmochim. Acta 49, 993–1000.

Cline, J.D., 1969. Spectrophotometric determination of hydrogen sulfide in natural waters. Limnol. Oceanogr. 14, 454–458.

Dando, P.R., Hughes, J.A., Leahy, Y., Niven, S.J., Taylor, L.J., Smith, C., 1995. Gas venting rates from submarine hydrothermal areas around the island of Milos, Hellenic Volcanic Arc. Cont. Shelf Res. 15, 913–929.

Dando, P.R., Thomm, M., Arab, H., Brehmer, M., Hooper, L., Jochimsen, B., Schlesner, H., Stohr, R., Miquel, J.-C., Fowler, S., 1998. Microbiology of shallow hydrothermal sites off Palaeochori Bay, Milos (Hellenic Volcanic Arc). Cah. Biol. Mar. 39, 369–372.

Dando, P.R., Stüben, D., Varnavas, S.P., 1999. Hydrothermalism in the Mediterranean Sea. Prog. Oceanogr. 44, 333–367.

Dick, G.J., Lam, P., 2015. Omic approaches to microbial geochemistry. Elements 11, 403–408.

Druschel, G.K., Baker, B.J., Gihring, T.M., Banfield, J.F., 2004. Acid mine drainage biogeochemistry at Iron Mountain, California. Geochem. Trans. 5, 13.

Falter, J.L., Sansone, F.J., 2000. Hydraulic control of pore water geochemistry within the oxic-suboxic zone of a permeable sediment. Limnol. Oceanogr. 45 (3), 550–557.

Fike, D.A., Grotzinger, J.P., 2008. A paired sulfate-pyrite $\delta^{34}S$ approach to understanding the evolution of the Ediacaran-Cambrian sulfur cycle. Geochim. Cosmochim. Acta 72, 2636–2648.

Fike, D.A., Grotzinger, J.P., 2010. Reconstructing biogenic pyrite burial in evaporite basins: an example from the Ara Group, Sultanate of Oman. Geology 38, 371–374.

Fike, D.A., Grotzinger, J.P., Pratt, L.M., Summons, R.E., 2006. Oxidation of the Ediacaran Ocean. Nature 444, 744–747.

Fike, D.A., Bradley, A.S., Rose, C.V., 2015. Rethinking the Ancient Sulfur Cycle. Ann. Rev. Earth Planet. Sci. 43, 20.1–20.30.

Fike, D.A., Houghton, J., Moore, S.E., Gilhooly III, W.P., Dawson, K., Druschel, G.K., Amend, J.P., Orphan, V.J., 2017. Spatially resolved capture of hydrogen sulfide from the water column and sedimentary pore waters for abundance and stable isotopic analysis. Mar. Chem. 197, 26–37.

Fischer, W.W., Fike, D.A., Johnson, J.E., Raub, T.D., Guan, Y., Kirschvink, J.L., Eiler, J.M., 2014. SQUID–SIMS is a useful approach to uncover primary signals in the Archean sulfur cycle. Proc. Natl. Acad. Sci. 111, 5468–5473.

Fram, J.P., Pawlak, G.R., Sansone, F.J., Glazer, B.T., Hannides, A.K., 2014. Miniature thermistor chain for determining surficial sediment porewater advection. Limnol. Oceanogr. Methods 12 (4), 155–165.

Fry, B., Ruf, W., Gest, H., Hayes, J.M., 1988. Sulfur isotope effects associated with oxidation of sulfide by O_2 in aqueous solution. Chem. Geol. 73, 205–210.

Fytikas, M., Innocenti, F., Kolios, N., Manetti, P., Mazzuoli, R., Poli, G., Rita, F., Villari, L., 1986. Volcanology and petrology of volcanic products from the island of Milos and neighboring islets. J. Volcanol. Geotherm. Res. 28, 297–317.

Gilhooly, W.P., Fike, D.A., Druschel, G.K., Price, R.E., Amend, J.P., 2014. Sulfur and oxygen isotope insights into sulfur cycling in shallow-sea hydrothermal vents. Geochem. Trans. 15, 12.

Gilhooly, W.P., III, Reinhard, C.T., Lyons, T.W., 2016. A comprehensive sulfur and oxygen isotope study of sulfur cycling in a shallow, hyper-euxinic meromictic lake. Geochim. Cosmochim. Acta 189, 1–23.

Gill, B.C., Lyons, T.W., Young, S.A., Kump, L.R., Knoll, A.H., Saltzman, M.R., 2011. Geochemical evidence for widespread euxinia in the Later Cambrian ocean. Nature 469, 80–83.

Glud, R.N., 2008. Oxygen dynamics of marine sediments. Mar. Biol. Res. 4, 243–289.

Godelitsas, A., Price, R.E., Pichler, T., Amend, J., Gamaletsos, P., Göttlicher, J., 2015. Amorphous As-sulfide precipitates from the shallow water hydrothermal vents off Milos Island (Greece). Mar. Chem. 177, 687–696.

Gomes, M.L., Fike, D.A., Bergmann, K., Knoll, A.H., 2017. Environmental insights from high-resolution (SIMS) sulfur isotope data in multiple generations of sulfides in Proterozoic microbialites with diverse mat textures. Geobiology 16, 17–34.

Hurtgen, M.T., Arthur, M.A., Halverson, G.P., 2005. Neoproterozoic sulfur isotopes, the evolution of microbial sulfur species, and the burial efficiency of sulfide as sedimentary pyrite. Geology 33, 41–44.

Jensen, S.I., Kuhl, M., Glud, R.N., Jorgensen, L.B., Prieme, A., 2005. Oxic microzones and radial oxygen loss from roots of *Zostera marina*. Mar. Ecol. Prog. Ser. 293, 49–58.

Johnston, D.T., Farquhar, J., Canfield, D.E., 2007. Sulfur isotope insights into microbial sulfate reduction: when microbes meet models. Geochim. Cosmochim. Acta 71, 3929–3947.

Jones, D.S., Fike, D.A., 2013. Dynamic sulfur and carbon cycling through the end-Ordovician extinction revealed by paired sulfate-pyrite δ^{34}S. Earth Planet. Sci. Lett. 363, 144–155.

Kafantaris, F.C., 2017. On the Reactivity of Nanoparticulate Elemental Sulfur: Experimentation and Field Observations. Doctoral dissertation. University-Purdue University Indianapolis, Indiana.

Kaplan, I.R., Rittenberg, S.C., 1964. Microbiological fractionation of sulphur isotopes. Microbiology 34, 195–212.

Leavitt, W.D., Halevy, I., Bradley, A.S., Johnston, D.T., 2013. Influence of sulfate reduction rates on the Phanerozoic sulfur isotope record. PNAS 110, 11244–11249.

Lloyd, R.M., 1968. Oxygen Isotope Behavior in the Sulfate-Water System. J. Geophys. Res. 73, 6099.

Luther, G.W., Glazer, B.T., Ma, S., Trouwborst, R.E., Moore, T.S., Metzger, E., ... Taillefert, M., 2008. Use of voltammetric solid-state (micro) electrodes for studying biogeochemical processes: laboratory measurements to real time measurements with an in situ electrochemical analyzer (ISEA). Mar. Chem. 108, 221–235.

Meyer-Dombard, D.R., Amend, J.P., Osburn, M.R., 2013. Microbial diversity and potential for arsenic and iron biogeochemical cycling at an arsenic rich, shallow-sea hydrothermal vent (Tutum Bay, Papua New Guinea). Chem. Geol. 348, 37–47.

Mills, H.J., Kiel Reese, B., Shepard, A., Dowd, S.E., Riedinger, N., Morono, Y., Inagaki, F., 2012. Characterization of metabolically active bacterial populations in subseafloor Nankai Trough sediments above, within, and below the sulfate–methane transition zone. Front. Microbiol. 3, 113.

Mizutani, Y., Rafter, T.A., 1969. Oxygen isotopic composition of sulphates – part 4. NZ J. Sci. 12, 60–68.

Nomikou, P., Papanikolaou, D., Alexandri, M., Sakellariou, D., Rousakis, G., 2013. Submarine volcanoes along the Aegean volcanic arc. Tectonophysics 597–598, 123–146.

Pichler, T., Giggenbach, W.F., McInnes, B.I.A., Buhl, D., Duck, B., 1999. Fe sulfide formation due to seawater-gas-sediment interaction in a shallow-water hydrothermal system at Lihir Island, Papua New Guinea. Econ. Geol. 94, 281–288.

Price, R.E., Giovannelli, D., 2017. A Review of the Geochemistry and Microbiology of Marine Shallow-Water Hydrothermal Vents.

Price, R.E., Savov, I., Planer-Friedrich, B., Bühring, S.I., Amend, J., Pichler, T., 2013. Processes influencing extreme as enrichment in shallow-sea hydrothermal fluids of Milos Island, Greece. Chem. Geol. 348, 15–26.

Rickard, D., Luther, G.W., 2007. Chemistry of iron sulfides. Chem. Rev. 107, 514–562.

Rickard, D., Morse, J.W., 2005. Avid-Volatile Sulfide (AVS). Marine Chemistry. vol. 97. pp. 141–197.

Rozan, T.F., Theberge, S.M., Luther III, G., 2000. Quantifying elemental sulfur (S_0), bisulfide (HS^-) and polysulfides (S_x^{2-}) using a voltammetric method. Anal. Chim. Acta 415, 175–184.

Rusch, A., Amend, J.P., 2008. Functional characterization of the microbial community in geothermally heated marine sediments. Microb. Ecol. 55, 723–736.

Schloss, Patrick D., Westcott, Sarah L., Ryabin, Thomas, Hall, Justine R., Hartmann, Martin, Hollister, Emily B., Lesniewski, Ryan A., et al., 2009. Introducing mothur: open-source, platform-independent, community-supported software for describing and comparing microbial communities. Appl. Environ. Microbiol. 75 (23), 7537–7541.

Sievert, S.M., Brinkhoff, T., Muyzer, G., Ziebis, W., Kuever, J., 1999. Spatial Heterogeneity of Bacterial Populations along an Environmental Gradient at a Shallow Submarine Hydrothermal Vent near Milos Island (Greece). Appl. Environ. Microbiol. 65, 3834–3842.

Sim, M.S., Ono, S., Donovan, K., Templer, S.P., Bosak, T., 2011. Effect of electron donors on the fractionation of sulfur isotopes by a marine *Desulfovibrio* sp. Goechimica et Cosmochimica Acta. 75, 4244–4259.

Slowey, A.J., Marvin-Dipasquale, M., 2012. How to overcome inter-electrode variability and instability to quantify dissolved oxygen, Fe (II), Mn (II), and S (− II) in undisturbed soils and sediments using voltammetry. Geochem. Trans. 13, 6.

Strauss, H., 1999. Geological evolution from isotope proxy signals - sulfur. Chem. Geol. 161, 89–101.

Turchyn, A.V., Brüchert, V., Lyons, T.W., Engel, G.S., Balci, N., Schrag, D.P., Brunner, B., 2010. Kinetic oxygen isotope effects during dissimilatory sulfate reduction: a combined theoretical and experimental approach. Geochim. Cosmochim. Acta 74, 2011–2024.

Valsami-Jones, E., Baltatzis, E., Bailey, E.H., Boyce, A.J., Alexander, J.L., Magganas, A., Anderson, L., Waldron, S., Ragnarsdottir, K.V., 2005. The geochemistry of fluids from an active shallow submarine hydrothermal system: Milos Island, Hellenic Volcanic Arc. J. Volcanol. Geoth. Res. 148, 130–151.

Varnavas, S.P., Cronan, D.S., 2005. Submarine hydrothermal activity off Santorini and Milos in the Central Hellenic Volcanic Arc: a synthesis. Chem. Geol. 224, 40–54.

Wenzhöfer, F., Holby, O., Glud, R.N., Nielsen, H.K., Gundersen, J.K., 2000. In situ microsensor studies of a shallow water hydrothermal vent at Milos, Greece. Mar. Chem. 69, 43–54.

Wilson, M.B., Zhang, C., Gandhi, J., 2011. Analysis of inorganic nitrogen and related anions in high salinity water using ion chromatography with tandem UV and conductivity detectors. J. Chromatogr. Sci. 49, 596–602.

Wing, B.A., Halevy, I., 2014. Intracellular metabolite levels shape sulfur isotope fractionation during microbial sulfate respiration. Proc. Natl. Acad. Sci. 111, 18116–18125.

Yücel, M., Sievert, S.M., Vetriani, C., Foustoukos, D.I., Giovannelli, D., Le Bris, N., 2013. Eco-geochemical dynamics of a shallow-water hydrothermal vent system at Milos Island, Aegean Sea (Eastern Mediterranean). Chem. Geol. 356, 11–20.